Title: Alkene Hydrosilylation on Oxide-supported Pt-ligand Single-site Catalysts

Authors: Linxiao Chen; Iyad S. Ali; George E. Sterbinsky; Jocelyn T. L. Gamler; Sara E. Skrabalak; Steven L Tait

To be cited as: 10.1002/cctc.201900530

Link to VoR: https://doi.org/10.1002/cctc.201900530

For submission to ChemCatChem

Alkene Hydrosilylation on Oxide-supported Pt-ligand Single-site Catalysts

Linxiao Chen,[a] Iyad S. Ali,[a] George E. Sterbinsky,[b] Jocelyn T. L. Gamler,[a] Sara E. Skrabalak,[a] and Steven L. Tait*[a]

[a] L. Chen, I. S. Ali, J. T. L. Gamler, Prof. S. E. Skrabalak, Prof. S. L. Tait

Department of Chemistry

Indiana University

800 E. Kirkwood Ave., Bloomington, Indiana 47405 (U. S. A.)

E-mail: tait@indiana.edu

[b] Dr. G. E. Sterbinsky

Advanced Photon Source,

Argonne National Laboratory

9700 S. Cass Ave., Lemont, Illinois 60439 (U. S. A.)

Abstract

Heterogeneous single-site catalysts (SSCs), widely regarded as promising next-generation catalysts, blend the easy recovery of traditional heterogeneous catalysts with desired features of homogeneous catalysts: high fraction of active sites and uniform metal centers. We previously reported the synthesis of Pt-ligand SSCs through a novel metal-ligand self-assembly method on MgO, CeO_2, and Al_2O_3 supports (*J. Catal.* **2018**, *365*, 303-312). Here, we present their applications in the industrially-relevant alkene hydrosilylation reaction, with 95% yield achieved under mild conditions. As expected, they exhibit better metal utilization efficiency than traditional heterogeneous Pt catalysts. The comparison with commercial catalysts (Karstedt and Speier) reveals several advantages of these SSCs: higher selectivity, less colloidal Pt formation, less alkene isomerization/hydrogenation, and better tolerance towards functional groups in substrates. Despite some leaching, our catalysts exhibit satisfactory recyclability and the single-site structure remains intact on oxide supports after reaction. Pt single-sites were proved to be the main active sites rather than colloidal Pt formed during the reaction. An induction period is observed in which Pt sites are activated by Cl detachment and replacement by reactant alkenes. The most active species likely involves temporary detachment of Pt from ligand or support. Catalytic performance of Pt SSCs is sensitive to the ligand and support choices, enabling fine tuning of Pt sites. This work highlights the application of heterogeneous SSCs created by the novel metal-ligand self-assembly strategy in an industrially-relevant reaction. It also offers a potential catalyst for future industrial hydrosilylation applications with several improvements over current commercial catalysts.

Introduction

Catalytic hydrosilylation, the addition of silicon hydrides (**2**, Scheme 1) (Si−H bonds) to multiple bonds (particularly C=C or C≡C bonds, **1**), has been one of the most important reactions in silicon chemistry. Since its first report in 1947,[1] hydrosilylation has been extended to a broad range of unsaturated substrates. It has been widely applied in industry to functionalize silicone polymers and other silica-based materials, to produce diverse materials with desired physiochemical properties.[2] These functionalized materials are of paramount importance in manufacturing diverse commodities, such as resins, lubricant oils, and coatings.[3] Catalytic hydrosilylation itself is also an efficient method to create silica-containing polymers as preceramic,[4] adhesive,[5] and sealing materials.[6] Furthermore, the cross-linking between multi-hydride and multi-vinyl silicone polymers provides a technology for silicone curing (elastomers, coatings).[3a, 7] Aside from heavy application in polymer industry, catalytic hydrosilylation of silane monomers also attracts significant interests, as it is a versatile synthetic tool to generate Si−C building blocks in fine chemical synthesis.[8]

Most industrial hydrosilylation processes use homogeneous Pt complex catalysts. In the late 1950s, Speier discovered that the $H_2PtCl_6/^{i}Pr-OH$ system (**13**) is an effective hydrosilylation catalyst with vastly improved selectivity.[9] It was the most commonly used industrial catalyst, until being replaced by the more active and selective Karstedt catalyst and its derivatives. The Karstedt catalyst (**14**), a platinum(0) complex containing vinyl-siloxane ligands that was initially reported in 1973,[10] is still the benchmark for hydrosilylation activity. Other metals, such as Rh, Ir, Fe, Ru, Ni, Ti, and Re,[11] as well as non-metal catalyst (boron/phosphorus-based)[12] have also been explored due to concerns with the use of Pt, including side reactions (selectivity), high cost, volatile market, and uncertainty in the future supply of Pt. However, none of these alternatives

have been able to match the hydrosilylation activity of Pt, so it seems likely that the industry will largely rely on Pt catalysts for a considerable amount of time. Current investigations remain focused on improving Pt-based catalysts, aiming to develop more efficient and stable catalysts with lower cost.[13]

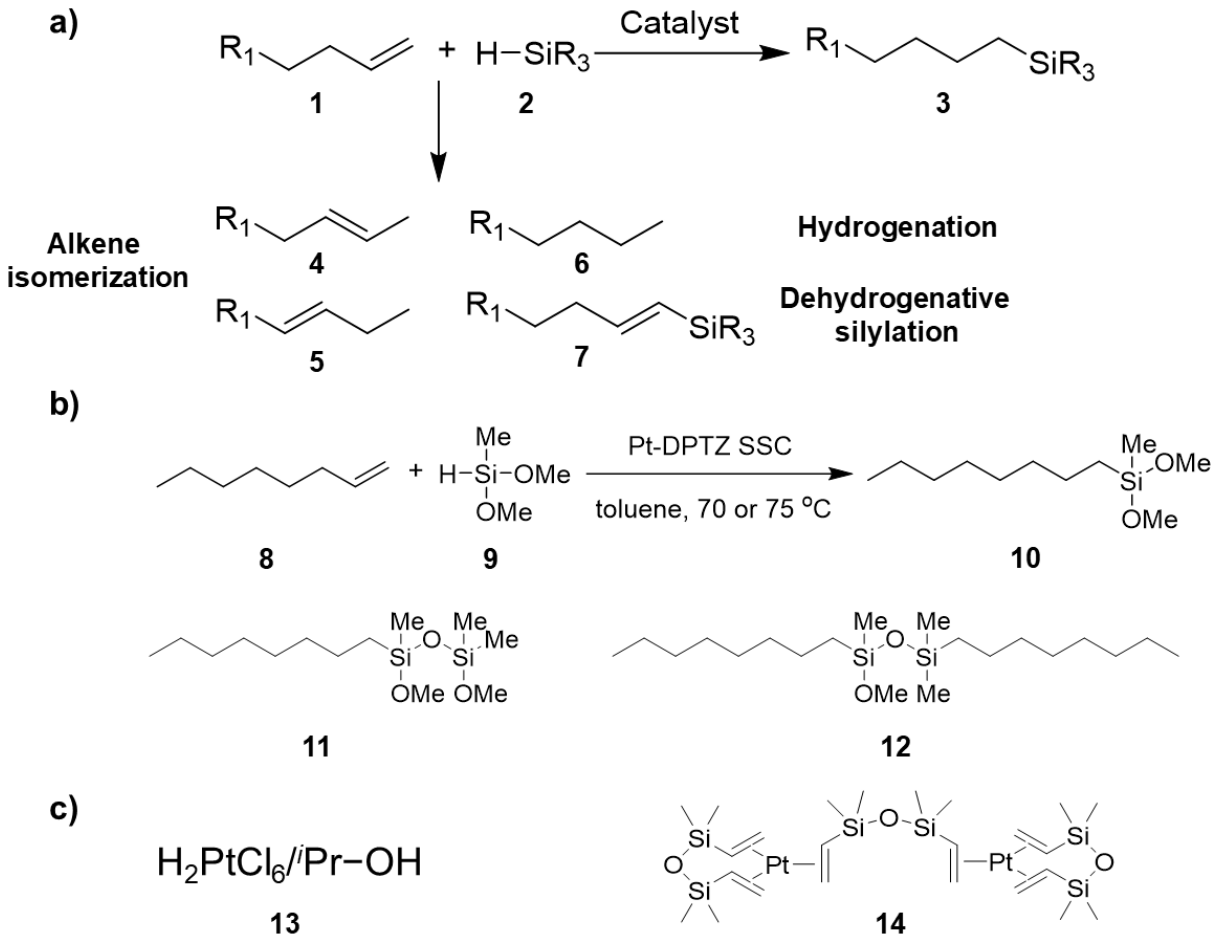

Scheme 1. Alkene hydrosilylation reactions and catalysts. **(a)** General representation of alkene hydrosilylation reactions and potential side reactions. A wide variety of side chains can be selected for the silane positions (R, not necessarily all the same) and alkene (R_1) to design the desired propoerties of the final product. **(b)** The hydrosilylation reaction performed in this work between 1-octene (**8**) and dimethoxymethyl silane (**9**), as well as the main Si-containing byproducts detected by GC-MS (**11**, **12**). **(c)** Structures of the Speier (**13**) and Karstedt (**14**) catalysts (commercial homogeneous catalysts).

Drawbacks of current commercial catalysts include the aggregation of Pt centers into colloids and multiple side reactions from C=C bonds. Despite some reports stating that colloidal Pt also catalyze hydrosilylation,[14] the dominant opinion is that Pt aggregation leads to deactivation.[3a, 15] Most Pt catalysts also catalyze alkene isomerization, hydrogenation, and dehydrogenative silylation reactions that yield byproducts **4-7**. Recently, motivated by the early work of Marko, *et al.*, with N-heterocyclic carbene,[13a, 13b] platinum-carbene complexes have been explored extensively as potential replacements that provide better stability.[16] Other endeavors include trinuclear Pt(0) catalysts with alkyne ligands,[17] and anti-sulfur-poisoning Pt catalysts.[18] Heterogeneous Pt catalysts have been applied to this reaction as well, including Pt(0) nanoparticles,[14] PtO_2,[13c] and supported Pt single-sites.[19] The initial mechanism model for alkene hydrosilylation was proposed by Chalk and Harrod in 1965, and has enjoyed great acceptance since then (Figure S1).[20] The oxidative addition of silane occurs first on Pt centers, and then C=C bond coordinates with Pt. The migratory insertion of C=C bonds to Si−H bonds and the subsequent reductive elimination from Pt eventually yield products. A modified Chalk-Harrod mechanism was later proposed including the insertion of unsaturated substrates to Pt−Si bond,[21] but has been shown recently to be unfavorable to the original Chalk-Harrod mechanism.[22]

Heterogeneous single-site catalysts (SSCs) have attracted attentions across the catalysis community as a strategy to combine advantages of homogeneous and heterogeneous catalysts.[23] SSCs have a large fraction of active sites (ideally 100% dispersion) and offer the potential for high selectivity due to the uniform character of the metal centers, as in organometallic homogeneous catalysts, while offering characteristics of heterogeneous catalysts for convenient

separation. SSCs have proved effective in gas phase and solution phase reactions, including hydrosilylation ($Pt^{\delta+}/TiO_2$ and Pt/graphene SSCs).[19a, 19b, 24]

Previous work from our group established a novel SSC synthesis strategy using metal-ligand self-assembly on powdered oxide supports.[25] The development of these systems was based on well-controlled model systems on single crystal surfaces in ultra-high vacuum.[26] On multiple powdered oxide supports, Pt can be atomically dispersed in oxidized Pt(II) form between N binding pockets, stabilized by the oxidizing ability of the 3,6-Di-2-pyridyl-1,2,4,5-tetrazine (DPTZ) ligand (Figures 1a, 1b).[25]

In this work, we report detailed investigations into alkene hydrosilylation using these oxide-supported Pt-DPTZ SSCs. Satisfactory yield was achieved under mild conditions for several catalytic cycles, with higher activity per Pt site than traditional nanoparticle catalysts. Compared with commercial catalysts, supported Pt-DPTZ SSCs are not only easier to recycle, but also provide higher yield, less colloidal Pt, fewer byproducts from alkene, and improved tolerance to epoxy groups in substrates. The evolution of Pt single-sites, including leaching from the support to aggregate into colloidal Pt in solution during the reaction as well as active site formation during the induction period or pretreatment, was systematically explored to better understand Pt behavior during catalysis. This is the first report using SSCs synthesized from the metal-ligand self-assembly strategy for industrially relevant reactions. Their effectiveness in alkene hydrosilylation catalysis and improvements over current commercial catalysts offer practical advantages.

Results and Discussions

1. **Catalytic performance of Pt-DPTZ single-site catalysts (SSCs).** The synthesis of oxide-supported Pt-DPTZ SSCs was previously reported by our group.[25] Pt(II) single-sites were created using metal-ligand self-assembly, taking advantage of the favorable N binding pockets in DPTZ (Figure 1a) and its electron-accepting potential that stabilizes isolated Pt cations. The simultaneous impregnation of Pt precursor $H_2PtCl_6 \cdot 6H_2O$ and DPTZ onto MgO, CeO_2, or Al_2O_3 powders generated Pt-DPTZ single-site structures (Figure 1b, details of the synthesis procedure are provided in the Experimental section), in which Pt also interacts with O from oxide supports (not shown in drawing). The single-site nature of Pt was confirmed by the extended X-ray absorption fine structure (EXAFS) region of X-ray absorption spectroscopy (XAS, Figure 1c) and other techniques (Figure S2). X-ray photoemission spectroscopy (XPS) shows that > 90% Pt sites exist as Pt(II) complexes, and the formation of metallic Pt nanoparticles (NP, zero valent) or mixed Pt(IV) oxide (on MgO) are almost completely prevented (Figure 1d). These results point to the formation of a structure like that in Figure 1b, similar to what has been reported in analogous model systems,[26] although the formation of some PtO_xCl_y single-sites may also be possible, especially on CeO_2, a vacancy-abundant oxide support.

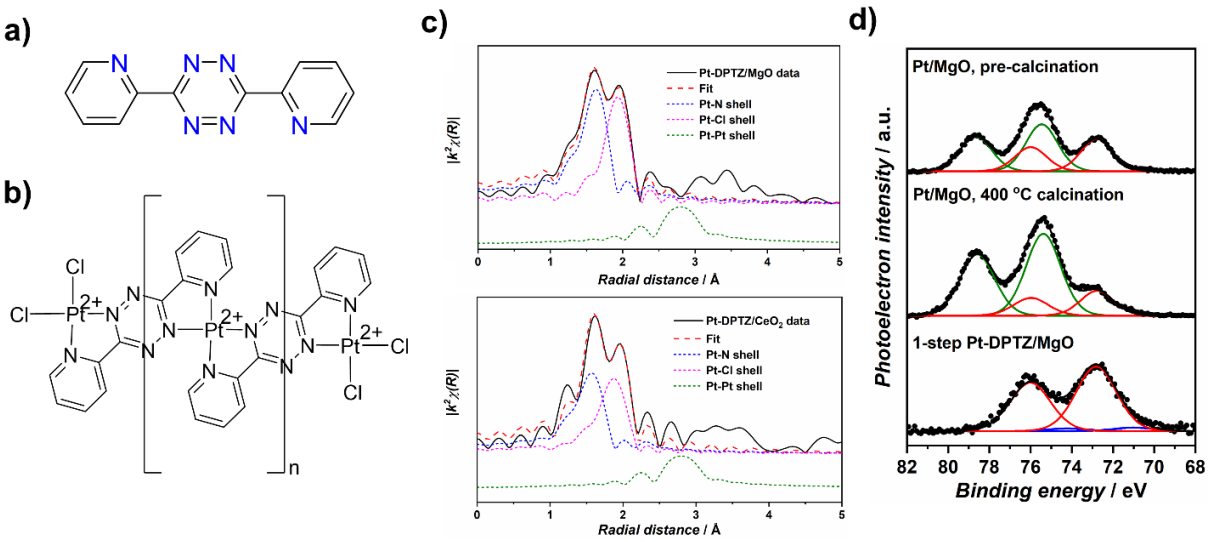

Figure 1. A summary of synthesis and characterization of oxide-supported Pt-DPTZ SSCs. **(a)** Structure of DPTZ. **(b)** Proposed structure of Pt-DPTZ single-site complex chains on oxide supports, with Pt binding to surface O from the bottom or at chain ends omitted. **(c)** First-shell EXAFS fittings of Pt-DPTZ/MgO (top) and Pt-DPTZ/CeO_2 (bottom) showing the absence of Pt–Pt shell. **(d)** Pt 4f XPS fittings showing on Pt-DPTZ/MgO, almost all Pt sites are of +2 oxidation states, with little metallic Pt(0) nanoparticles or mixed Pt(IV) oxide (Mg_2PtO_4) formation. Reprinted from reference [25], with permission from Elsevier.

Table 1. Catalytic performance of Pt-DPTZ SSCs and other catalysts in the hydrosilylation reaction between 1-octene **8** and dimethoxymethyl silane **9**.

Entry	Catalyst	*T* (°C)	*t* (min)	Yield[1] (%)	Pt concentration (ppm)	TON per Pt[2] (× 10^3)
1	Pt-DPTZ/MgO[3]	75	120	95	10	cc
2	Pt-DPTZ/MgO[3]	70	30	44	10	9.0
3	Pt(NP)/MgO	70	30	4	81	0.2
4	Mg_2PtO_4/MgO	70	30	47	87	1.1
5	Pt-DPTZ/CeO_2[3]	70	30	91	16	cc
6	Pt-DPTZ/CeO_2	60	20	51	16	6.5
7	Pt(NP)/CeO_2	60	20	73	40	3.7
8	Pt-DPTZ/Al_2O_3[3]	70	30	85	32	cc
9	Karstedt catalyst[3]	70	30	86	16	cc
10	Speier catalyst[3]	70	30	13	16	cc

All reactions were performed with 3 mmol **8**, 2.5 mmol **9**, and 1.5 mL toluene (solvent).
[1] Yield values reported here are GC-MS values based on **9** because excess **8** (1.2 eq) was used.
[2] TON per Pt values are presented to compare activity and only calculated if **9** was not completely converted (cc).
[3] Data in these entries are reproduced from reference [25].

Table 1 shows that oxide-supported Pt-DPTZ SSCs are highly effective catalysts for the hydrosilylation reaction between 1-octene (**8**, Scheme 1) and dimethoxymethylsilane (**9**). Reactions were performed using 1.2 eq. of **8** due to unavoidable side reactions involving C=C bonds. C=C isomerization products 2-octene, 3-octene, and hydrogenation product octane were all identified by gas chromatography–mass spectrometry (GC-MS). 100% conversion of **9** was achieved with Pt-DPTZ SSCs under mild conditions (75 °C, 2 h on MgO, and 70 °C, 30 min on CeO_2 and Al_2O_3, entry 1, 5, and 8) at low Pt concentrations (< 35 ppm). GC yield of main

product from anti-Markovnikov addition, **10** (calculated from **9**), is satisfactory (95% on MgO, 91% on CeO_2, and 85% on Al_2O_3) and is comparable with or higher than both commercial homogeneous catalysts (86% on Karstedt catalyst and 13% on Speier catalyst). Major Si-containing byproducts detected by GC-MS are dimers **11** and **12**, and no Markovnikov addition products are observed. Pt-DPTZ SSC performance is support-dependent: only 50% silane conversion is observedon MgO, while 100% conversion is observed on CeO_2 or Al_2O_3 under the same conditions (Table 1, entries 2, 5, and 8). This partially originates from the lower Pt loading on MgO (0.09 wt% compared with 0.35 wt% on CeO_2 and 0.7 wt% on Al_2O_3). Nevertheless, the turnover number per Pt value (TON per Pt) on Pt-DPTZ/MgO at 70 °C in 30 min (9×10^3, entry 2) is only approximately 1.5 times of that on Pt-DPTZ/CeO_2 at 60 °C in 20 min (6.5×10^3, entry 6), indicating that activity per Pt site is also affected by metal-support interactions. A non-supported (homogeneous) version of Pt-DTPZ was not be tested due to poor solubility in toluene. Average TOF values calculated by dividing TON per Pt by reaction time (5.4 s^{-1} at 60 °C, Table 1, entry 6) are significantly higher than previously reported values on other Pt SSCs, $Pt^{\delta+}/TiO_2$ (< 0.21 s^{-1} at 90 °C) and Pt/graphene (0.5 s^{-1} at 60 °C) at the same or even higher temperature,[19a, 19b] showing the superiority of our Pt-DPTZ system. We note that metallic Pt NP are almost catalytically inactive when supported on MgO (entry 3). CeO_2-supported Pt NP do exhibit activity, but the TON per Pt is lower than that on Pt-DPTZ/CeO_2 SSC (3.8×10^3 in entry 7 compared with 6.5×10^3 in entry 6) with the same reaction time and temperature. Similarly, Mg_2PtO_4/MgO (the stable bulk mixed oxide phase obtained after depositing Pt solely onto MgO and calcination under air, entry 4) is active, but with a lower TON per Pt than Pt-DPTZ/MgO SSC (entry 2) with the same reaction time and temperature. This is possibly due to one crucial advantage SSCs have over traditional metal aggregate catalysts: the fraction of active metal

centers is higher due to complete site isolation and uniform chemical environments. The sharply contrasting activity between MgO and CeO_2-supported Pt(0) NP again highlights impacts of metal-support interaction in this reaction, and reveals the complexity behind the unsolved controversy in existing literature about whether colloidal Pt(0) are active in this reaction or not.[3a, 14-15]

2. **Comparison of Pt SSCs with commercial catalysts.** *(a) Selectivity.* As hydrosilylation catalysts, Pt-DPTZ SSCs at surfaces show several advantages over commercial homogeneous catalysts (Karstedt and Speier). The heterogeneous nature of SSCs at surfaces is a preferred characteristic due to its easy separation, especially in small molecule synthesis. This advantage of heterogeneous catalysts is usually accompanied by relatively low selectivity due to non-uniform chemical environments of metal sites. Nonetheless, this trade-off is avoided in this system, as higher selectivity was achieved on Pt-DPTZ/MgO SSC (95%, entry 1 in Table 1) than on the Karstedt catalyst (86%, entry 9) at comparable temperatures (each reaction run to complete conversion to compare selectivities). On Pt-DPTZ/MgO, the selectivity benefits from the uniform structure of Pt sites, a unique feature of SSCs among heterogeneous catalysts. MgO surfaces may also have geometric restrictions on the adsorption and reaction of substrates on Pt sites, limiting undesired reaction pathways. On CeO_2 and Al_2O_3, the selectivity is slightly lower (91%, entry 5, and 85%, entry 8), potentially due to the co-existence of multiple types of Pt single-sites (such as PtO_xCl_y) at surface vacancies, but it is still comparable to the Karstedt catalyst (86%, entry 9) with the same reaction conditions and complete silane conversion. We note that the 86% yield on Karstedt catalyst reported here is close to and slightly higher than previous literature reports (78%) under almost identical conditions,[13a, 13b] so it is a reliable

reference. The heterogeneous nature of Pt-DPTZ SSCs also helps the selectivity by exempting the use of a co-solvent. On Speier catalyst, the low yield (13% in entry 10) is due to the exchange between methoxy groups in **9** or **10** and the co-solvent isopropanol, which does not exist when using Pt-DPTZ SSCs. We recognize that the 13% yield can be improved by using less isopropanol in catalyst preparation, but these side reactions are unavoidable.[9, 27]

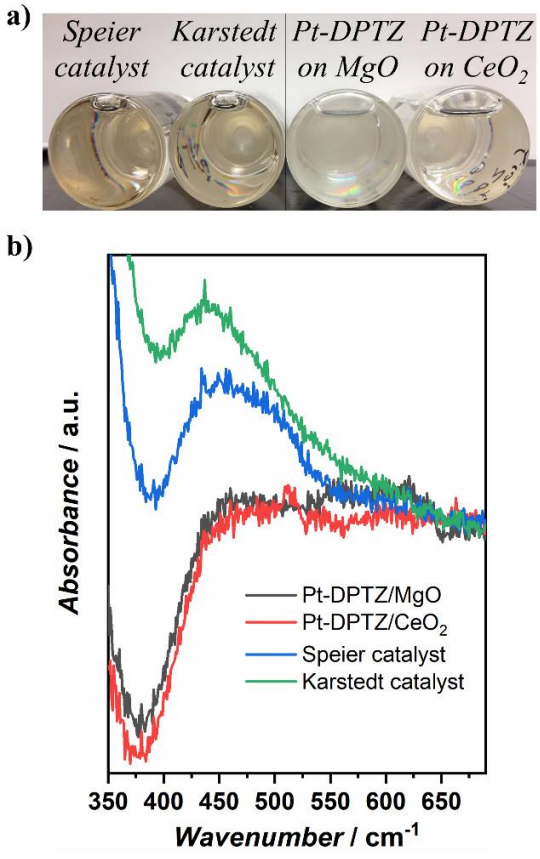

Figure 2. (a) A noticeable color difference between solutions of commercial Pt catalysts (left) and metal-ligand SSCs (right) indicates significantly less colloidal Pt formation for Pt-DPTZ SSCs than commercial Pt catalysts. From left to right: Speier catalyst, Karstedt catalyst, Pt-DPTZ/MgO, Pt-DPTZ/CeO_2. **(b)** UV-Vis spectra of post-reaction solutions exhibiting the 450-500 cm^{-1} absorption with commercial catalysts but not with SSCs. Absorption of toluene was subtracted from the raw spectra.

(b) Colloidal Pt formation. One major drawback from which the Karstedt catalyst suffers is the formation of colloidal Pt during the reaction, which is believed to cause side reactions and long-term deactivation.[3a, 15] Solutions were reported to gradually become yellow during the reaction,[13d, 28] and small Pt clusters were observed by microscopy after the reaction.[15a, 29] This problem is much less severe with Pt-DPTZ SSCs than commercial catalysts. A photo of post-reaction solutions using Pt-DPTZ/MgO, Pt-DPTZ/CeO_2, Speier catalyst, and Karstedt catalyst of the same Pt concentration is exhibited in Figure 2a. Solutions with both SSCs show significantly lighter yellow color than two commercial catalysts. The color observation is confirmed by UV-Vis spectra (Figure 2b), where solutions with both commercial catalysts have absorbance between 450 and 500 cm^{-1}, consistent with the yellow color. In contrast, solutions with Pt-DPTZ SSCs have negligible absorbance in this region, indicating less colloidal Pt formation. The four post-reaction solutions were centrifuged to collect any solid product and imaged by transmission electronic microscopy (TEM). SSC samples show smaller particles compared with large Pt black bulk formed from the commercial catalysts (Figure S3). Meanwhile, XPS and XAS on post-reaction Pt-DPTZ/SSCs show that Pt aggregation does not occur on surfaces (see next section), *i.e.*, there is no Pt aggregation on the surfaces during the reaction. During SSC-catalyzed reactions, only a fraction of Pt are leached into solutions (see next section), so the concentration of Pt vulnerable to aggregation is lower than commercial catalysts that are homogeneous. Furthermore, Pt leached off supports should also be more resistant to aggregation than Pt in commercial catalysts, as the favorable N binding pockets and oxidizing ability provided by DPTZ stabilize Pt(II) cations. In comparison, all ligands in Speier and Karstedt catalysts bind with Pt relatively weakly and do not offer sufficient oxidizing potential to prevent the reduction

of Pt (the Karstedt catalyst consists of zero valent Pt). Consequently, Pt(0) colloids are formed easily.

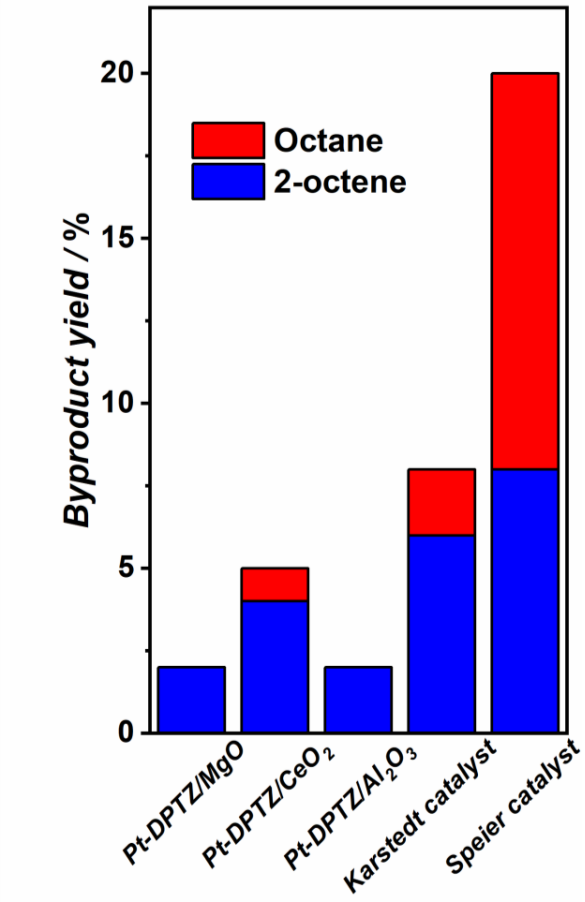

Figure 3. Comparison of byproducts yield from **8**, with blue bars showing isomerization product 2-octene yield, while red bars showing hydrogenation product octane yield.

(c) Alkene isomerization and hydrogenation. Two major side reactions in alkene hydrosilylation are isomerization and hydrogenation of the C=C bond, forming 2-octene/3-octene and octane from 1-octene (**8**), respectively. Figure 3 shows the yield of 2-octene and octane from **8** on Pt-DPTZ SSCs and commercial catalysts. These side reactions occur to a less extent on all Pt-DPTZ SSCs. Pt-DPTZ/CeO_2 generates the most byproducts among the three probably because of the abundant PtO_xCl_y single-sites at surface vacancies. We suspect that on

Pt-DPTZ SSCs, the isomerization is a branch from the hydrosilylation cycle. First, we discovered that **8** alone, without the presence of **9**, cannot be isomerized or hydrogenated, with or without colloidal Pt formed in hydrosilylation reaction. Besides, Figure S4 exhibits concentrations of 2-octene and 3-octene detected at various reaction times normalized to their post-reaction concentrations. The comparison of these two curves with the same curve for hydrosilylation product **10** reveals that time scales of isomerization and hydrosilylation are similar. After hydrosilylation stops due to the complete consumption of **9**, isomerization stops as well, despite an excess of **8** in solution. These observations are similar with results reported by Kuhn et al. on Karstedt catalyst,[15b] where they claimed that isomerization results from the migratory insertion step of the Chalk-Harrod hydrosilylation cycle (Figure S1), and its competition with hydrosilylation is determined by which carbon binds with Pt after the insertion. Although reaction mechanisms on Pt-DPTZ SSCs might differ from Karstedt catalyst, our observations imply the same conclusion: hydrosilylation and isomerization likely branch from the same catalytic cycle. Furthermore, some previous studies on Karstedt catalyst argued that colloidal Pt formed during the reaction, not the Pt complex, are mainly responsible for isomerization.[14a] Nevertheless, our results suggest this is not the case for Pt-DPTZ SSCs. If colloidal Pt were much more active in isomerization than Pt complexes, the byproduct formation would have been very slow relative to the formation of **10** at the initial stage due to a lack of colloidal Pt, and would accelerate as Pt aggregate gradually. However, in Figure S4, shapes of 2-octene and 3-octene curves are highly similar with that of the **10** curve, contradicting this theory. Our results suggest that isomerization and hydrosilylation mostly share the same active sites. Consequently, less byproduct formation on Pt-DPTZ SSCs cannot be explained by less colloidal Pt formation

shown above. Instead, it may be relevant with the presence of support surfaces making intermediates of side reactions less favorable electronically or sterically.

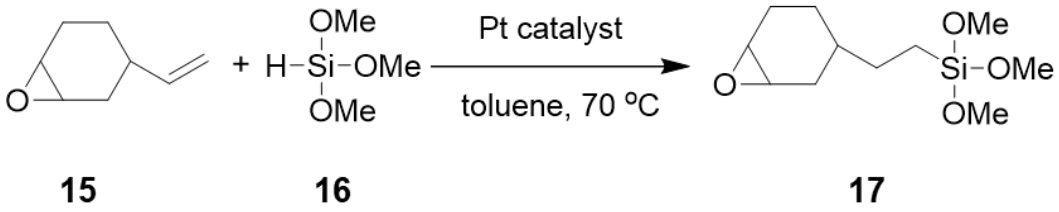

Scheme 2. Hydrosilylation reaction between 4-vinyl-1-cyclohexane 1,2-epoxide (**15**) and trimethoxysilane (**16**). Reaction conditions: 80 °C, 1 min, 16 ppm Pt, 2.5 mmol **16**, 3 mmol **15**, and 1.5 mL toluene as solvent.

(d) Tolerance with epoxy group. Another advantage of Pt-DPTZ SSCs over commercial catalysts is their tolerance towards the epoxy group in substrates. Hydrosilylation with epoxy-containing substrates is particularly important in Si-polymer industry because the epoxy group provides desirable physiochemical properties to products.[2d, 30] Unfortunately, Karstedt catalyst has been known to show low selectivity in these reactions, as it catalyzes undesired ring-opening side reactions.[13a, 13b] Our experiments show similar results: a 52% yield of desired product (**17**, Scheme 2) in the reaction involving epoxy-containing alkene (**15**) at 100% silane (**16**) conversion. This number is also consistent with previous reports (< 50%).[13a, 13b] No major byproducts from ring-opening reactions were detected by GC-MS, so we suspect that reactants go through ring-opening polymerization, as suggested in prior studies.[31] The yield of **17** further drops to 17% when no solvent was used, supporting the idea that main side reactions are intermolecular. Pt-DPTZ SSCs show obvious improvement over Karstedt catalyst regarding this problem: 71%, 64%, and 60% **17** yields were achieved when supported on CeO_2, Al_2O_3, and MgO, respectively. The electronic and geometric modifications provided by supports likely suppress side reactions in these cases, although this may not necessarily be true for other

substrates. As with commercial catalysts and most other homogeneous catalysts,[3a, 3b, 15b, 32] SSCs do not show any hydrosilylation activity when internal alkenes such as 2-octene are used.

3. Evolution of Pt sites during catalysis. *(a) Stability of Pt single-sites.* We examined the stability and recyclability of Pt-DPTZ SSCs. Table 2 shows characterization results of MgO- and CeO_2-supported Pt-DPTZ SSCs before and after catalysis (with 100% **9** conversion). Pt wt% measurements by inductively coupled plasma mass spectrometry (ICP-MS, Table 2, first row) show that both SSCs suffer from Pt leaching, which is less severe on CeO_2 (32%) than on MgO (67%). The ICP-MS values are consistent with the Pt : Ce or Pt : Mg ratio calculated from XPS (last row in Table 2). The leaching was confirmed by the presence of Pt in post-reaction solutions measured by ICP-MS. Nonetheless, the average TON on each Pt site during the reaction is around 8000, so the leaching probability during one turnover cycle is actually small. Stirring Pt-DPTZ/MgO in pure solvent (toluene) at reaction temperature without **8** or **9** led to 50% Pt leaching, indicating that the natural solvent-thermal instability of Pt-DPTZ single-sites, instead of hydrosilylation turnovers, accounts for most of the leaching from the MgO support. No significant binding of DPTZ to these supports is observed without Pt,[25] thus, the main attractive force to hold Pt-DPTZ complexes on surfaces are Pt-support interactions.[25] Therefore, the difference in Pt stability on CeO_2 and MgO supports reflects a difference in the strength of Pt-support interactions, which has been known to be stronger on CeO_2. Pt-DPTZ/Al_2O_3 was also evaluated, which shows 50% Pt leaching after catalysis. We will focus on CeO_2 and MgO supports in the following experiments because CeO_2 offers the best Pt stability while Pt leached from MgO was the most concentrated, promoting analysis. Despite leaching, Figure 4 shows that Pt-DPTZ/CeO_2 can be recycled four times with high yield of **10**, after which the yield decreases gradually.

Table 2. XPS analysis of MgO- and CeO_2-supported Pt-DPTZ SSC before and after hydrosiylaltion catalysis.

	Pt-DPTZ/CeO_2		Pt-DPTZ/MgO	
	Fresh	Used	Fresh	Used
Pt loading (wt%)[1]	0.35	0.24	0.09	0.03
Pt 4$f_{2/7}$ binding energy (eV)	72.7	72.8	72.8	72.6
Pt(II) fraction[2]	> 0.9	0.9	0.9	0.7
Pt(0) fraction	< 0.1	0.1	0.1	0.3
DPTZ : Pt[3]	0.47	0.47	0.73	0.75
Cl : Pt[3]	0.98	0.55	0.92	1.01
Pt : Ce or Pt : Mg[3]	0.16	0.10	0.049	0.015

[1] Pt loading values were calculated from ICP-MS measurements.
[2] Pt(IV) have not been observed with meaningful quantity on any samples.
[3] DPTZ : Pt (or Cl : Pt) ratios were calculated using XPS peak area of N 1*s* (or Cl 2*p*) region and Pt 4*f* region. Pt : Ce (CeO_2) or Pt : Mg (MgO) ratios were calculated using area of Pt 4*f* and Ce 3*d* or Mg 2*s* regions.

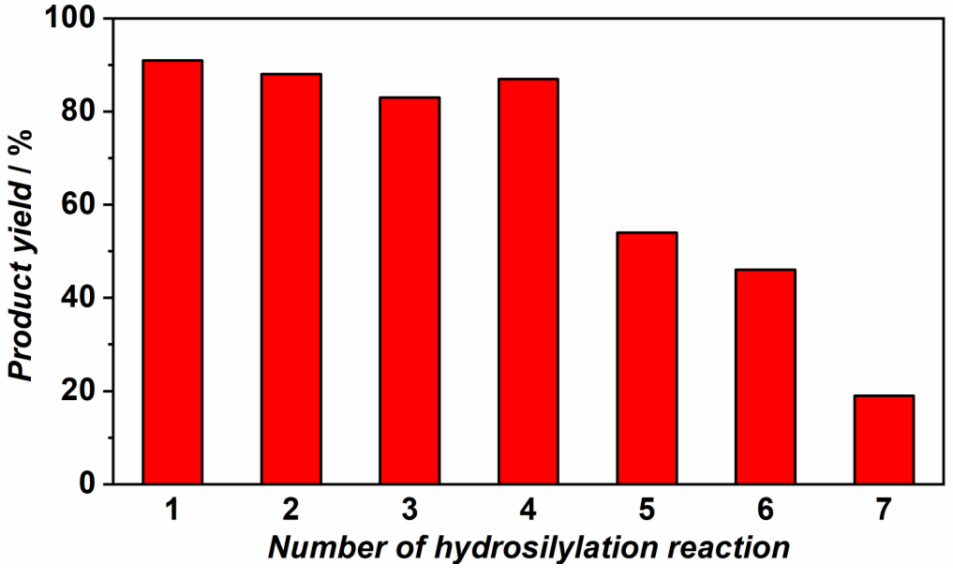

Figure 4. Recycliability test of Pt-DPTZ/CeO_2 SSC. Reaction conditions: 70 °C, 20 min, 15 mg catalyst. After each run, solid catalysts were separated from the solution by centrifuge and reused in the next.

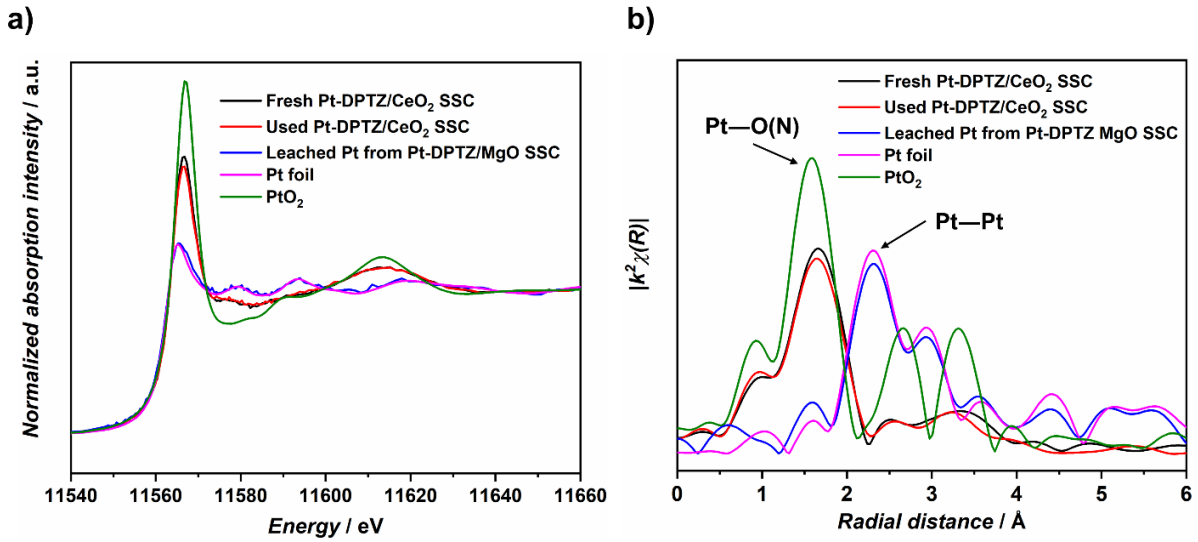

Figure 5. Pt *L*3-edge XAS of fresh (black) and used (red) Pt-DPTZ/CeO_2 SSC, Pt leached during catalysis from Pt-DPTZ/MgO SSC (blue), Pt foil standard (purple), and PtO_2 standard (green). **(a)** XANES region after normalization. **(b)** Fourier transform magnitudes of EXAFS region in *R*-space.

The structure of Pt sites after catalysis was revealed by XAS and XPS. *R*-space EXAFS (Figure 5b) at the Pt *L*3 edge of post-reaction Pt-DPTZ/CeO_2 SSC (red) exhibits similar features with its fresh form (black). A Pt—Pt shell is not observed, proving that recycled CeO_2-supported Pt retain their single-site character after catalysis. As shown in our prior work, all first-shell intensities in the fresh catalyst are fit well by contributions from the Pt—O(N) shell (~1.6 Å) and the Pt—Cl shell (~1.9 Å).[25] XPS data indicate a decrease in Cl concentration after the reaction, but there is not a noticeable change in EXAFS data (Figure 5b, red), which may be due to the formation of Pt—Si (~1.85 Å) or Pt—C bonds (with C=C π coordination, ~1.75 Å) after the loss of Cl. Close examination of the Pt *L*3 X-ray absorption near edge structure (XANES) region (Figure 5a) reveals that the white line intensity does not change significantly before and after reaction. White line intensity in normalized XANES spectra often positively correlates with metal oxidation states because it represents transitions from core orbitals to unfilled valence orbitals. In this case, the white line intensity remains between that of Pt foil (purple curve) and PtO_2 (green curve) standards, indicating that the Pt oxidation state is between 0 and +4. Previous XPS results show Pt exist as Pt(II) single-sites before catalysis,[25] so the Pt oxidation state remains close to +2 after catalysis. We also performed XAS on post-reaction solution containing Pt leached from Pt-DPTZ/MgO (Figure 5b, blue), to verify the formation of colloidal Pt in solution suggested by the yellow color (Figure 2a) and TEM images (Figure S3). We note that in the case of Pt-DPTZ/CeO_2, the amount of leached Pt is too small to analyze by XAS. As expected, Pt leached from Pt-DPTZ/MgO shows a strong Pt—Pt shell and a white line intensity close to Pt foil, consistent with Pt(0) colloids. Other scattering paths from adsorbates on colloidal Pt or from soluble Pt single-sites are too weak compared with the Pt—Pt shell to be detected by EXAFS, suggesting that the vast majority of leached Pt exists in relatively large Pt colloids.

These results prove that Pt aggregation does occur, but exclusively in solution, not on supports. These conclusions are further supported by XPS results in Table 2. Compared with fresh catalysts, Pt $4f_{2/7}$ binding energy of Pt-DPTZ SSCs does not change significantly after catalysis, and most Pt still exist in +2 oxidation states (peak fittings results see Figure S5). We note that on MgO, although the fraction of Pt(0) appears to increase after the reaction (Figure S5a), the amount of Pt(0) stays almost constant after considering the decrease of total Pt content. The apparent increase in Pt(0) fraction is simply a result of Pt(II) leaching. The DPTZ : Pt ratio on used catalysts is similar with that on fresh ones, implying the coordination between DPTZ and Pt does not change significantly either. A decrease in Cl : Pt ratio was observed on CeO_2, as some Cl might leave Pt during the reaction and then be replaced by reactants and/or products.

(b) Active species: single-sites or colloids? Considering the non-negligible Pt leaching and Pt aggregation in solution, it is necessary to question whether it is the colloidal Pt that is the catalytically active Pt species. The same question has been discussed on Karstedt catalyst in previous literature.[13d, 15, 28-29] Earlier studies supported colloidal Pt as active species,[28b, 29] but most recent work rejected this theory.[15] Our work also indicates that the colloidal Pt is not the main active species in our Pt-DPTZ SSC systems.

After a reaction that converted **9** completely (70 °C for 30 min or 75 °C for 2 h when supported by CeO_2 or MgO, respectively), the solution/solid mixture was centrifuged at a speed that keeps all colloidal Pt in the solution (details in SI). The separated solid and solution were then each used as catalysts in separate experiments to conduct a second reaction at the same temperature, but for much shorter time (3 min on CeO_2 or 30 min on MgO). Centrifugation at room temperature was used instead of hot filtration because of the reversible detachment of Pt

during the reaction (discussed in detail below). Table 3 shows that a 17% yield was achieved on recycled Pt-DPTZ/CeO_2, compared with only 4% on the colloidal Pt in solution. For comparison, fresh Pt-DPTZ/CeO_2 yielded 19% **10** in the first 3 min. Note that in the first 3 min reaction with fresh catalyst, the concentration of colloidal Pt is much lower than that in the post-reaction solution because they form gradually as the reaction proceeds. Therefore, turnovers on colloidal Pt in this 3 min should be responsible for significantly less than 4% **10** yield, which is only 1/5 of the 19% total **10** yield. We conclude that despite the possibility that colloidal Pt might be an active hydrosilylation catalyst, most turnovers occur on Pt single-sites. When TON per Pt values are used for comparison, it is also clear that colloidal Pt are much less active in the first 3 min (1.5×10^3) than Pt single-sites (2.4×10^3 in the first run and 3.2×10^3 in the second). On MgO, despite more severe Pt leaching and less active Pt single-sites, Pt single-sites still show higher activity per Pt in the second run (TON per Pt = 13.0×10^3) than colloidal Pt (9.5×10^3). We note that, despite the indication by EXAFS that in post-reaction solutions (after removing the solid material) most Pt exist as colloidal Pt, we cannot eliminate the presence of soluble Pt single-sites, which may contribute to the turnovers.

Table 3. Performances of CeO_2- and MgO-supported Pt-DPTZ SSCs at various state.

Support	Reaction condition	Catalyst state	Yield (%)	TON per Pt ($\times 10^3$)
CeO_2	70 °C, 3 min	Fresh	19	2.4
		Recycled[1]	17	3.2
		Post-reaction solution[1]	4	1.5
		Fresh, pre-treated by 1-octene[2]	38	4.8
MgO	75 °C, 30 min	Fresh	44	9.0
		Recycled[1]	21	13.0
		Post-reaction solution[1]	31	9.5

All reaction were performed with 3 mmol **8**, 2.5 mmol **9**, and 1.5 mL toluene as solvent. MgO reactions were performed with 25 mg catalyst; CeO_2 reactions were performed with 15 mg catalyst.
[1] The first reaction before these reactions were performed at 70 °C, 30 min (CeO_2) or at 75 °C, 2 h (MgO). After the reaction, solid and solution were separated by centrifuge.
[2] Pretreatments with 1-octene were conducted at the reaction temperature for 30 min.

(c) Structure of Pt at different stages of hydrosilylation. The results above indicate that Pt single-sites are the main active species and that they remain isolated on these surfaces after catalysis. However, the most active form of Pt seems to be different from the ideal structure shown in Figure 1b because of the induction period observed on Pt-DPTZ/CeO_2. Figure 6 presents the yield of **10** with reaction time on Pt-DPTZ/CeO_2, showing a clear acceleration during the first 3 min. Reaction rate then drops due to the consumption of reactants. Previous studies on Karstedt and Speier catalyst also reported induction periods, which some attribute to ligand exchange processes.[9-10, 15b] On both supports, the recycled Pt-DPTZ SSCs exhibit higher TONs per Pt in the corresponding reaction time (3.2×10^3 on CeO_2, 13.0×10^3 on MgO) than fresh ones (2.4×10^3 on CeO_2, 9.0×10^3 on MgO). This also indicates the presence of an

induction period: the recycled catalyst has been activated during the first run and thus catalyzes more turnovers in the second run during the initial stage of the reaction.

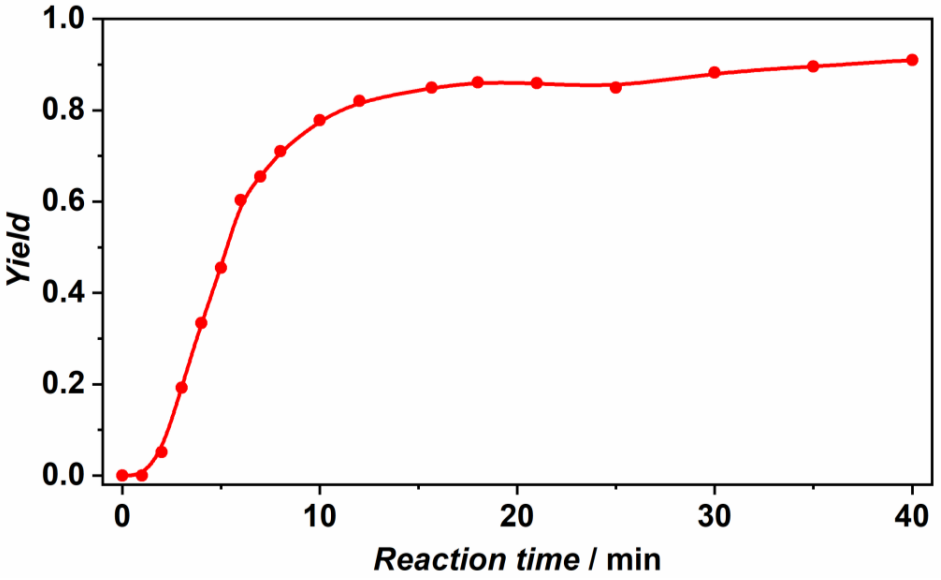

Figure 6. Yield of hydrosilylation product **10** with reaction time on Pt-DPTZ/CeO_2 SSC. The acceleration in reaction rate at the beginning indicates an induction period. The differential form of this figure, showing the rate vs. time is presented as Figure S6.

Since colloidal Pt are less active than Pt single-sites, the induction period cannot be explained by the formation of colloidal Pt. Previous reports linked the induction period on the Karstedt catalyst with the coordination of Pt sites with reactant alkene.[15] We found that pre-treating Pt-DPTZ/CeO_2 SSC with 1-octene at the reaction temperature before the reaction enhances the initial activity of Pt-DPTZ/CeO_2 by a factor of 2 (Table 3, with a yield increase from 19% to 38% in the first 3 min, and a TON per Pt increase from 2.4×10^3 to 4.8×10^3). In contrast, pretreatments with hydrosilylation-resistant 2-octene or reactant silane **9** do not have this effect. We also noticed that with Pt-DPTZ/CeO_2, the Cl : Pt ratio drops by half after catalysis

(Table 2), implying Cl detachment from Pt during catalysis. This is intuitive as Cl atoms are typically regarded as good leaving groups in organometallic chemistry.

We also performed *in situ* XAS to further investigate the structure of active sites. The reaction was performed under the same condition as Figure 6, but quenched at 1, 2, 5, and 10 min by placing the reaction tube into a dry ice bath, allowing us to detect the chemical environment of Pt at various stages of the reaction by XAS. In these experiments, Pt coordination environments are complicated by the presence of Pt−Si and Pt−C bonds from intermediates and the spectra quality is limited by the extremely low Pt concentration in the reaction mixture (~10-20 ppm), so a rigorous quantitative fitting with multiple shells is not possible, but we analyze these qualitatively. Figure 7a shows that after 2 min reaction, when the induction period is almost complete (according to Figure 6 and S6), the intensity at ~1.9 Å (Pt−Cl) drops, and the first-shell peak shifts to shorter distance compared with fresh catalyst. This is consistent with the loss of Pt−Cl coordination from XPS results. Figure 7a also shows that similar changes occur during the 1-octene pre-treatment, indicating that the shorter induction period due to pre-treatment is also due to Cl loss.

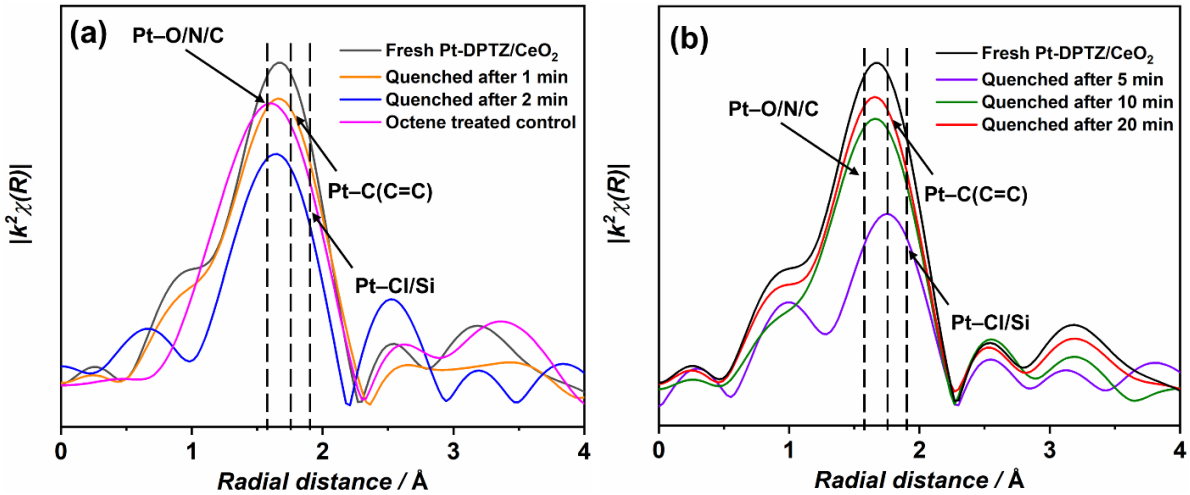

Figure 7. Pt *L*3-edge XAS (EXAFS region in *R*-space, k^2-weighted) of Pt-DPTZ/CeO_2 SSC at various stages of the hydrosilylation reaction. Panel **(a)** shows fresh (black), quenched after 1 min (orange) and 2 min (blue) of reaction, and collected *in situ* (70 °C) under 1-octene treatment. Panel **(b)** shows fresh (black) and quenched after 5 min (purple), 10 min (green), and 20 min (red) of reaction. At 20 min, the reaction has run to completion.

Figure 7b compares the coordination environment of Pt when the turnover is fastest (5 min) and when the reaction is close to complete (10 min) with catalyst at the end of the reaction (20 min). EXAFS after 5 min reaction (purple) has a first-shell peak around 1.76 Å with significantly lower intensity than fresh catalyst, especially at ~1.6 Å. Considering the loss of Pt—Cl coordination during catalysis, this suggests more contribution from Pt—Si (~1.85 Å) and Pt—C π (~1.75 Å) bonds than Pt—O/N bonds (~1.6 Å). This is in sharp contrast with spectra from fresh catalyst (black curve) where the first-shell peak was located at 1.65 Å, which is from the combination of Pt—O/N bonds and Pt—Cl (~1.9 Å) bond. The peak position shift and intensity drop at 5 min indicate that after the induction period, the most active Pt species have less O and N coordination, implying that they are detached from DPTZ and CeO_2. As reaction completes

(10 min and 20 min, green and red, respectively), the first-shell peak shifts back toward 1.65 Å, suggesting the detachment is reversible. XPS on solid catalyst obtained from quenching after 5 min show a decrease in Pt content to 50% of its fresh form. However, after 30 min of reaction, 68% of the original Pt content is found on the solid catalyst. The DPTZ : Pt ratio is virtually unchanged in both of these measurements compared to fresh catalyst (Table 2), indicating that the reattachment of Pt restores it to the supported metal-ligand state.

The detachment of Pt from ligand and/or support is not surprising. Previous EXAFS analysis suggests that the coordination number of Pt on fresh SSCs is between 4 and 5.[25] Even after Cl leaves during the induction period, the Pt coordination shell is still crowded for the reaction to proceed with Chalk-Harrold (Figure S1) or similar mechanisms. None of the quenching spectra shown in Figure 7 have significant contribution from Pt−Pt bonds, so the formation of Pt colloids is minimal with Pt-DPTZ/CeO_2 SSC. We note that after 5 min, the shift of the first shell away from ~1.6 Å also suggests a low contribution of Pt−C σ bonds compared with Pt−Si or Pt−C π bonds. This is significant because it implies that regardless of the exact mechanism, the rate-determining step is not reductive elimination forming C−H bond (step III_{HS} in Figure S1).

Overall, our results depict a complicated picture of how Pt-DPTZ single-sites evolve during hydrosilylation catalysis. The initial coordination of reactant alkene and leaving of Cl from Pt complete the induction period. At the most active stage of the reaction, Pt single-sites likely detach temporarily from DPTZ or support to provide necessary coordination vacancies. As the reaction completes, most Pt are recovered by re-coordinating with DPTZ and support, with a small fraction of Pt remaining in solution. On-surface Pt are still single-sites after catalysis, while leached Pt aggregate into colloids that are less active than single-sites. Further details of the reaction mechanisms are the subject of ongoing studies.

4. **Impact of ligand and support on Pt activity.** The impact of the ligand environment on the activity of the metal center is an important aspect of organometallic catalysis. In order to explore this aspect in our system, we replaced DPTZ with PDO and BMTZ ligands (Figures 8a, 8b) on both supports (CeO_2 and MgO). Both ligands have at least two binding pockets, allowing the growth of Pt-ligand complexes similar with Pt-DPTZ. Table 4 shows that for all six Pt-ligand SSCs, the binding energy of Pt $4f_{2/7}$ XPS peak does not deviate significantly from 72.8 eV, suggesting that most Pt are Pt(II) single-sites. BMTZ has a stronger electron affinity (oxidizing potential) than DPTZ and leads to the formation of +3 metal centers with V in model systems (on single crystal metal supports in UHV),[26c] but similar systems with Pt prefer a mixed redox isomer of Pt(II)/Pt(0) over odd-electron Pt oxidation states.[33] Here, it is interesting that simultaneous impregnation of Pt and BMTZ onto CeO_2 and MgO powders generates mainly Pt(II), similar to DPTZ, due to the difference in support interaction. On each of the supports studied, we observed the trend that ligand:Pt and Cl:Pt ratios (XPS) are negatively correlated with each other, where a higher ligand:Pt ratio implies longer chain length (larger *n* in Figure 1b).

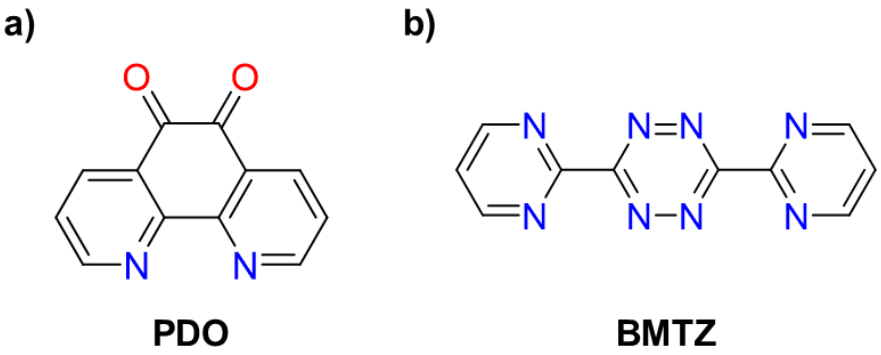

Figure 8. Structures of other ligands used in this work: **(a)** 1,10-phenanthroline-4,7-ketone (PDO). **(b)** Bis-pyrimidyltetrazine (BMTZ).

Table 4. Catalytic performances and XPS characterization results of Pt-ligand SSCs with various ligands on MgO and CeO_2.

Support	Ligand	Yield (%)	Pt loading (wt%)	TON per Pt ($\times 10^3$)	Pt $4f_{2/7}$ BE (eV)	Ligand : Pt	Cl : Pt
CeO_2 (60 °C, 20min)	DPTZ	51	0.34	5.4	72.9	0.47	1.56
	BMTZ	19	0.33	1.6	72.9	0.67	1.31
	PDO	29	0.81	1.3	72.9	1.03	1.17
MgO (75 °C, 30min)	DPTZ	68	0.09	8.6	72.8	0.73	0.92
	BMTZ	0	0.21	0.0	72.9	0.93	0.43
	PDO	53	0.05	10.7	72.3	0.37	1.03

All reaction were performed with 3 mmol **8**, 2.5 mmol **9**, and 1.5 mL toluene as solvent. MgO reactions were performed with 25 mg catalyst; CeO_2 reactions were performed with 15 mg catalyst.

Table 4 shows that the activity of Pt single-sites is highly sensitive to the choice of ligand and support. On both supports, Pt single-sites are most active when binding with DPTZ. The choice of ligand could be important for several reasons. First, on the same support, the activity measured by TON per Pt is positively correlated with Cl : Pt ratio. It is possible that the end-of-chain Pt that bind with Cl are more active because Cl is a better leaving group than DPTZ or support. Second, the distribution of Pt sites between outer surfaces and mesopores of the support depends on the ligand (see SI for details), which might affect activity too. Nonetheless, these two factors alone cannot explain the ligand dependence completely, as in the extreme case of Pt-BMTZ/MgO, no activity was observed despite the presence of Cl-bound Pt and a relatively high Pt loading compared with other ligands on MgO. We propose this is because Pt activity in this reaction is known to be sensitive to electronic structure, which is modified by the ligand. In homogeneous catalysis, ligand tuning offers an effective strategy to steer activity/selectivity of metal centers. Results here suggest that one can apply this powerful tool to metal-ligand SSCs.

This enables fine tuning electronic structures of metal centers, which is extremely difficult with traditional supported metal catalysts. Table 4 also highlights impacts of support again, as Pt activity also varies with the support when the same ligand is used. An oxide support is effectively a "heterogeneous ligand" that alters the electronic structures of Pt sites in a similar way with organic ligands; its surface structure also plays a role in determining the distribution of Pt sites: vacancy-abundant CeO_2 prevents the long-range growth of Pt-DPTZ chains, creating more end-of-chain sites and vacancy-trapped PtO_xCl_y sites. The porous structure of supports can affect the location of Pt sites. These factors all contribute to the activity of Pt. We are currently performing systematic investigation on support effects through defect engineering on oxide surfaces.

Conclusions

In this work, oxide-supported Pt-ligand SSCs synthesized by metal-ligand self-assembly are presented as highly effective heterogeneous catalysts for alkene hydrosilylation reactions. These SSCs provide unique advantages by combining the easy separation/recovery of heterogeneous catalysts with the high metal utilization efficiency/uniformity of homogeneous catalysts. Compared with current commercial catalysts, SSCs offer several advantages in easier catalyst recovery, improved selectivity, less colloidal Pt and alkene byproduct formation, as well as better tolerance towards epoxy groups in substrates. We found that Pt single-sites are leached into solution at a slow rate compared with reaction turnover. XAS and XPS show that leached Pt then aggregate into colloidal Pt that are much less active, while supported Pt remains as single-sites. Despite the leaching problem, Pt-DPTZ/CeO_2 SSC exhibits satisfactory recyclability. During the induction period, the coordination of Pt with reactant alkene and leaving of Cl are likely required

to activate Pt. DPTZ and support might reversibly detach from Pt at the most active stage to further provide coordination vacancies. We also discovered that the activity of Pt single-sites is sensitive to the choice of ligand and support. This might originate from the tuning of the electronic structure of Pt centers as well as the distribution of Pt on supports, and offers vast potentials for the fine tuning of metal single-sites.

Experimental section

Synthesis of supported Pt-ligand SSCs. The impregnation synthesis procedure of Pt-ligand SSCs has been described in detail in our previous publication.[25] For Pt-DPTZ on CeO_2: 0.0108 g (0.046 mol) DPTZ (Sigma Aldrich, 96%) were completely dissolved in 25 mL 1-butanol (Alfa Aesar, 99%) by stirring for 20 min at room temperature. 0.3 g CeO_2 (BET surface area ≈ 4.8 m^2/g) were added to the pink DPTZ solution and the mixture was then stirred for 2 h at room temperature. 0.0080 g $H_2PtCl_6 \cdot 6H_2O$ (Alfa Aesar, 99.95% metal basis, 0.015 mol, 1 wt% by Pt with respect to total catalyst mass; 3 eq. DPTZ with Pt) were dissolved in 5 mL 1-butanol. The Pt salt solution was then added to the MgO/DPTZ/1-butanol mixture dropwise under stirring within 30 min. The mixture was covered and stirred for 24 h, then dried at room temperature under dry air flow overnight. The dried catalyst was washed with water, then dichloromethane (DCM) until powders did not show any pink color (all free DPTZ removed). Al_2O_3- or MgO-supported SSCs were produced in the same way, except that CeO_2 powders were replaced by Al_2O_3 (ground to 60 mesh, BET surface area ≈ 195 m^2/g) or MgO (BET surface area ≈ 5.1 m^2/g) of the same mass. For PDO or BMTZ-bound SSCs, DPTZ was replaced by PDO (Sigma Aldrich, 98%) or BMTZ (synthesized by the group of Prof. Kenneth G. Caulton, Indiana University)[26c, 34] of the same mole quantity, and H_2O or acetone (VWR, ACS grade) were used to replace 1-

butanol as the solvent due to ligand solubility concerns. All metal SSCs were yellow or light yellow powders.

General procedures for alkene hydrosilylation reactions. The Karstedt catalyst used in this work was purchased from Sigma Aldrich (2% in xylene, diluted to 0.1% with toluene). The Speier catalyst was prepared by dissolving $H_2PtCl_6 \cdot 6H_2O$ in isopropanol (Macron, ACS grade) to make Pt concentration as 177 ppm. Pt catalysts (supported Pt SSCs or commercial catalysts) were weighed and kept in an empty reaction tube with cap. 2.5 mmol silane **9** (Alfa Aesar, > 97%) or **16** (Sigma Aldrich, 98%, mixture of isomers) and 3 mmol alkene **8** (Alfa Aesar, > 97%) or **15** (Sigma Aldrich, 98%) were weighed into another reaction tube, and 1.5 mL toluene (Macron, ACS grade) was added to the same tube. Both tubes were pre-heated in a water bath at the reaction temperature for 10 min, before reactants and solvent were added into the tube with Pt catalysts. The tube was capped during the reaction to avoid evaporation of silane with low boiling point. After the reaction, the tube was cooled down quickly with cold water flow, the solid catalysts were filtered out, and the liquid mixture was diluted for GC-MS measurements with an Agilent 6890N Gas Chromatograph and 5973 Inert Mass Selective Detector. Representative GC-MS spectra of a post-reaction solution and a standard solution used for calibration curves can be found as Figure S7-S8. Product yields were calculated from their response intensity (*m/z* = 203.2, 91.2, 83.2, and 85.2 for product **10**, **17**, 2-octene, and octane, respectively) in GC-MS with respect to the response of internal standard decane (Sigma Aldrich, > 99%, ~ 0.15 g added to all standard and post-reaction solutions to correct sampling volume errors) at *m/z* = 142.2 using pre-made calibration curves. A representative calibration curve is shown as Figure S9, exhibiting almost perfect linear relationship between normalized GC-MS response and concentration over the concentration range relevant to the experiments reported

here. For all samples we measured, the GC-MS response from decane is within ± 20% of standard solutions used in the calibration curves. All pure compounds for calibration curves were purchased from Sigma Aldrich. Use solid catalysts were collected for further characterization. The experiment measuring product yield at various reaction time was performed in a round-bottom flask with 10 times amount of catalysts, reactants, and solvent. At each reaction time, around 0.2 mL reactant mixture was taken out and shot into 10 mL toluene at room temperature immediately to ensure quick temperature drop. GC-MS measurements were then performed on each sample to measure product yields.

Characterization of Pt-ligand SSCs. XPS measurements were performed with a PHI Versaprobe II XP spectrometer using a monochromated Al X-ray source. A small amount of each powder sample was fixed onto a platen with double-sided tape. For CeO_2-supported samples, XPS were collected at Pt 4*f*, N 1*s*, C 1*s*, Cl 2*p*, Ce 3*d*, and O 1*s* regions. For MgO-supported samples, Mg 2*s* region was measured instead of Ce 3*d*. A neutralizer was used to alleviate surface charging. The binding energy was corrected with C 1*s* peak (284.8 eV) for MgO-supported samples, and Ce $3d_{5/2}$ main peak (882.4 eV) for CeO_2-supported samples. Details about XPS data processing are included in the SI.

Selected samples were characterized on JEOL JEM 1010 TEM which operated at 80 keV. Additional characterization with STEM was completed with JEOL JEM 3200FS operating at 300 keV. The TEM and STEM samples were prepared by centrifuging the post-reaction solutions to form a pellet from any solid product in the solutions. The collected solid was redispersed in a minimal amount of acetone and dropcast onto the TEM grid.

XAS measurements were performed at the 9-BM beamline at the Advanced Photon Source of Argonne National Laboratory. Solid samples were pressed into pellets with $d \approx 7$ mm and

solution samples were placed in a PEEK container with magnetic stirring to prevent Pt precipitation. The monochromatized X-ray energy was calibrated with the *L*3-edge of a Pt foil (11562.6 eV). X-ray absorption spectra were measured at the Pt *L*3-edge, from to 11363 to 12365 eV. For solid samples, both fluorescence and transmission data were collected and fluorescence data were used for analysis. For liquid samples, only fluorescence data were collected. XAS of a Pt foil, an α-PtO_2 pellet, and a K_2PtCl_6 pellet were measured as standard references; transmission data were used for analysis of standards. ICP-MS measurements were performed at IU Department of Earth & Atmospheric Sciences with an Agilent 7700 quadrupole ICP-MS instrument. Solid catalysts were treated with aqua regia to dissolve all Pt before measurement. For solution samples, the solvent was evaporated first and then the residue was treated with aqua regia to dissolve all Pt. UV-Vis spectra of post-reaction solutions were collected at IU Physical Biochemistry Instrumentation Facility with a Varian Cary 100 Bio UV/Visible Spectrometer. A cuvette was filled with each solution sample and toluene, and spectra were collected from 250 to 700 cm^{-1}. Absorption from toluene was subtracted from each spectrum to ensure the 600 – 700 cm^{-1} region is flat.

Acknowledgement

This work was supported by the U. S. Department of Energy, Office of Basic Energy Sciences, Chemical Sciences program, DE-SC0016367. XPS measurements were carried out at Indiana University (IU) Nanoscale Characterization Facility with assistance from Dr. Yaroslav Lasovyj. Access to XPS at the Nanoscale Characterization Facility was provided by the NSF Award DMR MRI-1126394. Transmission electron microscopy (TEM) imaging was performed at the IU Electron Microscopy Center. XAS measurements were performed at beamline 9-BM at the

Advanced Photon Source, a U. S. DOE Office of Science User Facility operated for the DOE Office of Science by Argonne National Laboratory under Contract No. DE-AC02-06CH11357. Dr. Xuemei Zhou assisted with XAS measurements. GC-MS measurements were carried out at the IU Mass Spectrometry Facility with assistance from Dr. Jonathan A. Karty.

Conflicts of interest

There are no conflicts of interest to declare.

Keywords: heterogeneous catalysis, single-site catalyst, hydrosilylation, platinum, X-ray photoelectron spectroscopy, X-ray absorption spectroscopy

References

[1] L. Sommer, E. Pietrusza, F. Whitmore, *J. Am. Chem. Soc.* **1947**, *69*, 188-188.

[2] aO. R. Pierce, Y. K. Kim, *Rubber Chem. Technol.* **1971**, *44*, 1350-1362; bH. Maciejewski, A. Wawrzyńczak, M. Dutkiewicz, R. Fiedorow, *J. Mol. Catal. A: Chem.* **2006**, *257*, 141-148; cB. Marciniec, E. Walczuk, P. Blazejewska-Chadyniak, D. Chadyniak, M. Kujawa-Welten, S. Krompiec, N. Auner, J. Weiss, *Wiley VCH, Weinheim* **2003**; dY. Morita, S. Tajima, H. Suzuki, H. Sugino, *J. Appl. Polym. Sci.* **2006**, *100*, 2010-2019; eE. Beyou, P. Babin, B. Bennetau, J. Dunogues, D. Teyssie, S. Boileau, *J. Polym. Sci., Part A: Polym. Chem.* **1994**, *32*, 1673-1681; fC. Iojoiu, M. J. Abadie, V. Harabagiu, M. Pinteala, B. C. Simionescu, *Eur. Polym. J.* **2000**, *36*, 2115-2123; gZ. Li, J. Qin, Z. Yang, C. Ye, *J. Appl. Polym. Sci.* **2004**, *94*, 769-774; hA. Sellinger, R. M. Laine, V. Chu, C. Viney, *J. Polym. Sci., Part A: Polym. Chem.* **1994**, *32*, 3069-3089; iD. B. Drazkowski, A. Lee, T. S. Haddad, D. J. Cookson, *Macromolecules* **2006**, *39*, 1854-1863; jA. Tuchbreiter, H. Werner, L. H. Gade, *Dalton Trans.* **2005**, 1394-1402.

[3] aD. Troegel, J. Stohrer, *Coord. Chem. Rev.* **2011**, *255*, 1440-1459; bB. Marciniec, *Hydrosilylation: a comprehensive review on recent advances, Vol. 1*, Springer Science & Business Media, **2008**; cT. Ganicz, T. Pakuła, W. A. Stańczyk, *J. Organomet. Chem.* **2006**, *691*, 5052-5055.

[4] aB. Boury, R. J. Corriu, D. Leclercq, P. H. Mutin, J. M. Planeix, A. Vioux, *Organometallics* **1991**, *10*, 1457-1461; bA. Mori, H. Sato, K. Mizuno, T. Hiyama, K. Shintani, Y. Kawakami, *Chem. Lett.* **1996**, *25*, 517-518.

[5] aM. J. O'brien, US Patent 6,531,540, **2003**; bC. Herzig, B. Deubzer, D. Huettner, US Patent 5,241,034, **1993**.

[6] aH. Jyono, H. Odaka, H. Ito, H. Iwakiri, US Patent 6,444,775, **2002**; bT. Watabe, T. Matsumoto, T. Onoguchi, K. Tsuruoka, US Patent 6,207,766, **2001**.

[7] P. Jerschow, *Silicone elastomers, Vol. 137*, Smart Publications, **2001**.

[8] aR. H. Morris, *Chem. Soc. Rev.* **2009**, *38*, 2282-2291; bB. K. Langlotz, H. Wadepohl, L. H. Gade, *Angew. Chem. Int. Ed.* **2008**, *47*, 4670-4674; cS. C. Bart, E. Lobkovsky, P. J. Chirik, *J. Am. Chem. Soc.* **2004**, *126*, 13794-13807; dI. Vankelecom, P. Jacobs, *Catal. Today* **2000**, *56*, 147-157.

[9] J. L. Speier, J. A. Webster, G. H. Barnes, *J. Am. Chem. Soc.* **1957**, *79*, 974-979.

[10] B. Karstedt, US Patent 3,775,452, **1973**.

[11] aM. Xue, J. Li, J. Peng, Y. Bai, G. Zhang, W. Xiao, G. Lai, *Appl. Organomet. Chem.* **2014**, *28*, 120-126; bM. Igarashi, T. Matsumoto, T. Kobayashi, K. Sato, W. Ando, S. Shimada, M. Hara, H. Uchida, *J. Organomet. Chem.* **2014**, *752*, 141-146; cH. Dong, Y. Jiang, H. Berke, *J. Organomet. Chem.* **2014**, *750*, 17-22; dJ. Y. Wu, B. N. Stanzl, T. Ritter, *J. Am. Chem. Soc.* **2010**, *132*, 13214-13216; eP. B. Glaser, T. D. Tilley, *J. Am. Chem. Soc.* **2003**, *125*, 13640-13641; fS. Nozakura, S. Konotsune, *Bull. Chem. Soc. Jpn.* **1956**, *29*, 326-331; gL. Bareille, S. Becht, J. L. Cui, P. Le Gendre, C. Moïse, *Organometallics* **2005**, *24*, 5802-5806; hS. Harder, J. Brettar, *Angew. Chem. Int. Ed.* **2006**, *45*, 3474-3478; iV. Leich, T. P. Spaniol, L. Maron, J. Okuda, *Chem. Commun.* **2014**, *50*, 2311-2314.

[12] aM. Rubin, T. Schwier, V. Gevorgyan, *J. Org. Chem* **2002**, *67*, 1936-1940; bM. Pérez, L. J. Hounjet, C. B. Caputo, R. Dobrovetsky, D. W. Stephan, *J. Am. Chem. Soc.* **2013**, *135*, 18308-18310.

[13] aI. E. Markó, S. Sterin, O. Buisine, G. Berthon, G. Michaud, B. Tinant, J. P. Declercq, *Adv. Synth. Catal.* **2004**, *346*, 1429-1434; bI. E. Markó, S. Stérin, O. Buisine, G. Mignani, P. Branlard, B. Tinant, J.-P. Declercq, *Science* **2002**, *298*, 204-206; cN. Sabourault, G. Mignani, A. Wagner, C. Mioskowski, *Org. Lett.* **2002**, *4*, 2117-2119; dL. N. Lewis, K. G. Sy, G. L. Bryant Jr, P. E. Donahue, *Organometallics* **1991**, *10*, 3750-3759; eB. Marciniec, J. Guliński, *J. Organomet. Chem.* **1993**, *446*, 15-23.

[14] aT. Galeandro-Diamant, M.-L. Zanota, R. Sayah, L. Veyre, C. Nikitine, C. de Bellefon, S. Marrot, V. Meille, C. Thieuleux, *Chem. Commun.* **2015**, *51*, 16194-16196; bB. P. Chauhan, J. S. Rathore, *J. Am. Chem. Soc.* **2005**, *127*, 5790-5791; cY. Bai, S. Zhang, Y. Deng, J. Peng, J. Li, Y. Hu, X. Li, G. Lai, *J. Colloid Interface Sci.* **2013**, *394*, 428-433.

[15] aJ. Stein, L. Lewis, Y. Gao, R. Scott, *J. Am. Chem. Soc.* **1999**, *121*, 3693-3703; bT. K. Meister, K. Riener, P. Gigler, J. r. Stohrer, W. A. Herrmann, F. E. Kühn, *ACS Catal.* **2016**, *6*, 1274-1284.

[16] aJ. C. Bernhammer, H. V. Huynh, *Organometallics* **2013**, *33*, 172-180; bJ. J. Dunsford, K. J. Cavell, B. Kariuki, *J. Organomet. Chem.* **2011**, *696*, 188-194; cM. A. Taige, S. Ahrens, T. Strassner, *J. Organomet. Chem.* **2011**, *696*, 2918-2927.

[17] B. Marciniec, K. Posała, I. Kownacki, M. Kubicki, R. Taylor, *ChemCatChem* **2012**, *4*, 1935-1937.

[18] C. M. Downing, H. H. Kung, *Catal. Commun.* **2011**, *12*, 1166-1169.

[19] aY. J. Chen, S. F. Ji, W. M. Sun, W. X. Chen, J. C. Dong, J. F. Wen, J. Zhang, Z. Li, L. R. Zheng, C. Chen, Q. Peng, D. S. Wang, Y. D. Li, *J. Am. Chem. Soc.* **2018**, *140*, 7407-7410; bY. Zhu, T. Cao, C. Cao, J. Luo, W. Chen, L. Zheng, J. Dong, J. Zhang, Y. Han, Z. Li, C. Chen, Q. Peng, D. Wang, Y. Li, *ACS Catal.* **2018**, *8*, 10004-10011; cH. Zai, Y. Zhao, S. Chen, L. Ge, C. Chen, Q. Chen, Y. Li, *Nano Res.* **2018**, *11*, 2544-2552; dQ. Li, S. Ji, M. Li, X. Duan, *Sci. China Mater.* **2018**, *61*, 1339-1344.

[20] A. J. Chalk, J. Harrod, *J. Am. Chem. Soc.* **1965**, *87*, 16-21.

[21] M. A. Schroeder, M. S. Wrighton, *J. Organomet. Chem.* **1977**, *128*, 345-358.

[22] aS. Sakaki, N. Mizoe, M. Sugimoto, *Organometallics* **1998**, *17*, 2510-2523; bS. Sakaki, N. Mizoe, M. Sugimoto, Y. Musashi, *Coord. Chem. Rev.* **1999**, *190*, 933-960.

[23] aZ. Huang, X. Gu, Q. Cao, P. Hu, J. Hao, J. Li, X. Tang, *Angew. Chem.* **2012**, *124*, 4274-4279; bE. Fako, Z. Lodziana, N. Lopez, *Catal. Sci. Technol.* **2017**, *7*, 4285-4293; cY. X. Chen, Z. W. Huang, Z. Ma, J. M. Chen, X. F. Tang, *Catal. Sci. Technol.* **2017**, *7*, 4250-4258.

[24] aH. Sohn, J. Camacho-Bunquin, R. R. Langeslay, P. A. Ignacio-de Leon, J. Niklas, O. G. Poluektov, C. Liu, J. G. Connell, D. Yang, J. Kropf, H. Kim, P. C. Stair, M. Ferrandon, M. Delferro, *Chem. Commun.* **2017**, *53*, 7325-7328; bW. Xu, Y. Li, B. Yu, J. Yang, Y. Zhang, X. Chen, G. Zhang, Z. Gao, *J. Solid State Chem.* **2015**, *221*, 208-215; cM. D. Marcinkowski, J. Liu, C. J. Murphy, M. L. Liriano, N. A. Wasio, F. R. Lucci, M. Flytzani-Stephanopoulos, E. C. H. Sykes, *ACS Catal.* **2016**, *7*, 413-420; dB. Hu, A. B. Getsoian, N. M. Schweitzer, U. Das, H. Kim, J. Nildas, O. Poluektov, L. A. Curtiss, P. C. Stair, J. T. Miller, A. S. Hock, *J. Catal.* **2015**, *322*, 24-37; eB. Qiao, A. Wang, X. Yang, L. F. Allard, Z. Jiang, Y. Cui, J. Liu, J. Li, T. Zhang, *Nat. Chem.* **2011**, *3*, 634-641; fH. Yan, H. Cheng, H. Yi, Y. Lin, T. Yao, C. Wang, J. Li, S. Wei, J. Lu, *J. Am. Chem. Soc.* **2015**, *137*, 10484-10487; gG. Vilé, D. Albani, M. Nachtegaal, Z. Chen, D. Dontsova, M. Antonietti, N. López, J. Pérez‐Ramírez, *Angew. Chem. Int. Ed.* **2015**, *54*, 11265-11269.

[25] L. Chen, G. E. Sterbinsky, S. L. Tait, *J. Catal.* **2018**, *365*, 303-312.

[26] aD. Skomski, C. D. Tempas, K. A. Smith, S. L. Tait, *J. Am. Chem. Soc.* **2014**, *136*, 9862-9865; bD. Skomski, C. D. Tempas, G. S. Bukowski, K. A. Smith, S. L. Tait, *J. Chem. Phys.* **2015**, *142*, 101913; cD. Skomski, C. D. Tempas, B. J. Cook, A. V. Polezhaev, K. A. Smith, K. G. Caulton, S. L. Tait, *J. Am. Chem. Soc.* **2015**, *137*, 7898-7902.
[27] J. L. Speier, in *Adv. Organomet. Chem., Vol. 17*, Elsevier, **1979**, pp. 407-447.
[28] aL. N. Lewis, R. J. Uriarte, N. Lewis, *J. Mol. Catal.* **1991**, *66*, 105-113; bL. N. Lewis, *J. Am. Chem. Soc.* **1990**, *112*, 5998-6004.
[29] aL. N. Lewis, N. Lewis, *J. Am. Chem. Soc.* **1986**, *108*, 7228-7231; bL. N. Lewis, R. J. Uriarte, *Organometallics* **1990**, *9*, 621-625.
[30] aW. Z. Wang, *Eur. Polym. J.* **2003**, *39*, 1117-1123; bS. Y. Feng, M. Z. Cui, *Reactive & Functional Polymers* **2000**, *45*, 79-83.
[31] aA.-L. Brocas, C. Mantzaridis, D. Tunc, S. Carlotti, *Prog. Polym. Sci.* **2013**, *38*, 845-873; bH. Sugimoto, C. Kawamura, M. Kuroki, T. Aida, S. Inoue, *Macromolecules* **1994**, *27*, 2013-2018; cE. N. Jacobsen, *Acc. Chem. Res.* **2000**, *33*, 421-431.
[32] B. Marciniec, *Comprehensive handbook on hydrosilylation*, Elsevier, **2013**.
[33] C. D. Tempas, D. Skomski, B. J. Cook, D. Le, K. A. Smith, T. S. Rahman, K. G. Caulton, S. L. Tait, *Chem. Eur. J.* **2018**, *24*, 15852-15858.
[34] W. Kaim, J. Fees, *Z. Naturforsch., B: Chem. Sci.* **1995**, *50*, 123-127.

Table of Contents entry

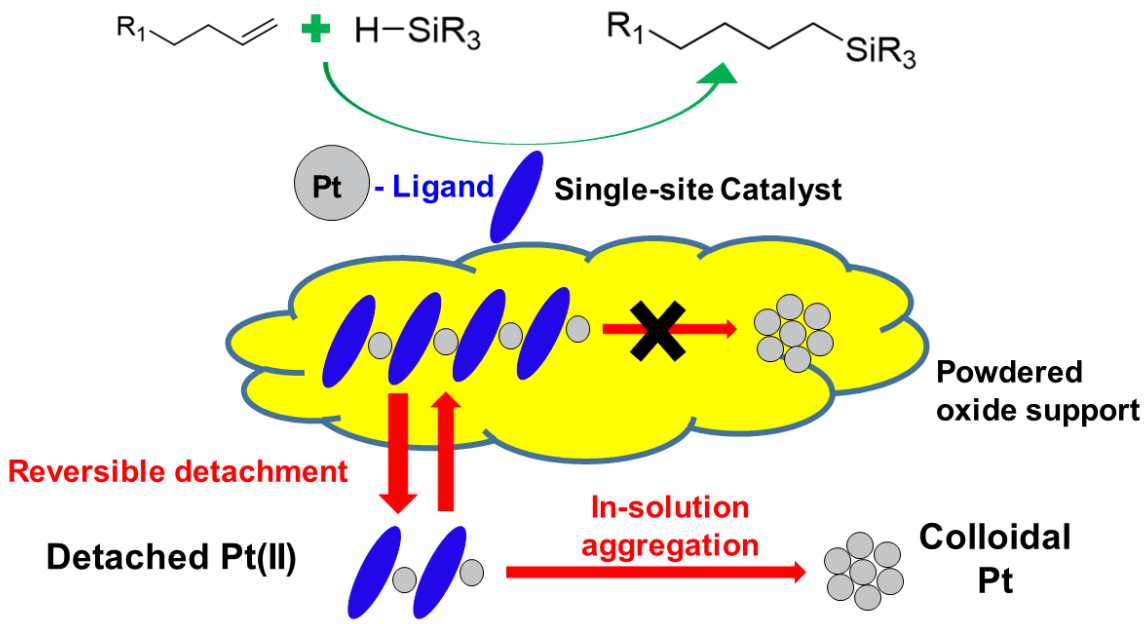

Supported Pt single-site catalysts developed for alkene hydrosilylation using a metal-ligand coordination strategy offer improvements over nanoparticle and commercial catalysts. Pt single-sites are the main active species, which require activation but do not aggregate on supports. Fine tuning of metal centers is demonstrated by varying the ligand and the powdered oxide support.